Indian Journal of Chemical Technology
Vol. 32, July 2025, pp. 518-533
DOI: 10.56042/ijct.v32i4.7191

Synthesis, characterization, anticorrosion properties, and theoretical study of two α-aminophosphonate derivatives

Samia Baatouche[1,2], Rachida Kerkour[1,3]*, Ouahiba Moumeni[3], Mouna Mehri[3,4], Nadjib Chafai[3] & Salah Chafaa[4]

[1]Département des sciences et techniques, Faculté de Science et Technologies, Université Abdelhafid Boussouf-Mila, BP 26 Mila, Algeria

[2]Unité de Recherche Valorisation des Resources Naturelles, Université des Frères Mentouri Constantine, Constantine, Algeria

[3]Laboratoire d'Electrochimie des Matériaux Moléculaires et Complexes (LEMMC), Université Ferhat Abbas Setif-1, El-Maabouda, 19000, Setif, Algeria

[4]Département de Sciences Agronomiques, Faculté des Sciences de la Nature et de la Vie et des Sciences de la Terre et de l'Univers, Université Mohamed El Bachir El Ibrahimi Bordj Bou Arréridj El-Anasser, 34030, Algeria

*E-mail: ayamanel2000@yahoo.fr

Received 8 December 2023; accepted 16 July 2025

Two α-aminophosphonates derivatives, namely Diethyl ((phenylamino)(pyridine-2-yl) methyl) phosphonate (o-DPAPMP) and Diethyl ((phenylamino)(pyridine-3-yl) methyl) phosphonate (m-DPAPMP), have been synthesised using the Kabachnik Fields reaction, and their structures have been confirmed through melting point, UV-visible absorption, FT-IR, and NMR (^{1}H, ^{13}C, ^{31}P) spectroscopy techniques. Their potential as anticorrosion agents for XC48 carbon steel in a 0.5 M H_2SO_4 solution are evaluated using various techniques, including weight loss measurements, Tafel polarization, electrochemical impedance spectroscopy, atomic force microscope, contact angle measurements, density functional theory (DFT), and molecular dynamics (MD). The results revealed that o-DPAPMP and m-DPAPMP exhibited inhibition efficiencies of 94.56% and 93.66%, respectively. The inhibition mechanism involved the adsorption of the inhibitors onto the metal surface via the Langmuir adsorption isotherm, with the energy-free standard values revealing both physical and chemical. AFM analyses demonstrated that both inhibitors prevented the normal functioning of carbon steel, with o-DPAPMP showing stronger inhibitory efficiency than m-DPAPMP. Contact angle measurements confirmed the surface's hydrophobic nature of the. Theoretical analyses using DFT and MD showed a strong correlation with experimental results.

Keywords: α-Aminophosphonates, Carbon steel, Corrosion inhibitors, DFT, Molecular dynamics

Introduction

Carbon steel accounts for approximately 85% of global annual steel production, with a consumption of around 700 million tons per year. It is the most widely used material in large quantities across various industries, including marine applications, nuclear power, fossil fuel power plants, petroleum production, chemical processing, refining, construction, and metal-processing equipment[1,2]. Despite its widespread use, carbon steel's main drawback is its limited resistance to corrosion in harsh environments. Corrosion significantly diminishes the material's effectiveness, leading to increased maintenance costs and lost production, which negatively impacts numerous industrial sectors. It is estimated that corrosion causes damage to about 150 million tons of steel annually, which represents roughly one-quarter of the total steel production worldwide[3]. Therefore, it is essential to protect steel and prevent corrosion. The use of inhibitors to protect the metal surface from acidic aggression has proven to be highly beneficial in various industries.

Studies have shown that organic compounds containing nitrogen, oxygen, sulfur, and phosphorus, as well as unsaturated bonds and conjugated systems, are effective inhibitors in various corrosive environments[4,5]. Among these, organophosphorus compounds have been particularly studied as inhibitors for metals and alloys in electrochemical settings due to their low cost, easy production, high purity, and low toxicity[6,7]. One important group of organophosphorus compounds is α-aminophosphonates, which are considered structural analogues of amino acids. These compounds are used in various applications, including industrial detergents and cleaners[8,9], as antioxidants agents[10], antitumor activity[11] and are increasingly being used as corrosion inhibitors[7-12]. One of the simplest methods for synthesizing these compounds is the Kabachnik–Fields reaction[13], a three-component organic reaction that produces α-aminophosphonates

from an amine, a carbonyl compound, and dialkyl phosphite. Several publications in recent years have documented the synthesis of α-aminophosphonates using this approach[12, 14].

Recently, computational chemistry techniques have been extensively applied to study organic compounds as corrosion inhibitors, helping to understand the relationship between their molecular structures and their inhibition effectiveness[5,6]. These methods calculate the electrical characteristics that are key to the inhibitory action. Additionally, molecular dynamic simulations are commonly used to analyze the adsorption of inhibitor molecules onto metal surfaces[7,15]. These simulations provide insights into how the inhibitor molecules adsorb to the metal surface and allow for the measurement of the adsorption energy between the organic inhibitor and the metal surface.

Given the importance of corrosion inhibitors in various industries, the present study aims to synthesize, characterize, and evaluate the inhibitory properties of two novel α-aminophosphonate derivatives based on pyridine in the ortho and meta positions. The focus is to investigate their corrosion inhibition performance on XC48 carbon steel in a 0.5 M H_2SO_4 medium. Atomic force microscopy (AFM) and contact angle measurements will be employed to examine the surface morphology and composition of XC48 carbon steel. These techniques will assess the hydrophilic and/or hydrophobic properties of the carbon steel samples protected from corrosion. Additionally, theoretical calculations and molecular dynamics simulations will be conducted to explore the relationship between the inhibitors' molecular structures and their inhibitory effectiveness.

Experimental Section

Material and solutions

The material used for corrosion study is carbon steel X48, which had the following composition (in weight percent): 0.50% C, 0.8% Mn, 0.40% Si, 0.10% Mo, 0.4% Ni, 0.40% Cr, 0.045% P, 0.045% S, with the remaining 95% being Fe. The aggressive solution consists of a freshly prepared 0.5 M H_2SO_4 solution, made for each experiment using distilled water and analytical-grade H_2SO_4 (97%). The inhibitor concentration range used in the study was between 10^{-6} and 10^{-3} M. All chemicals employed were purchased from Aldrich Chemical Company and were of high purity.

Synthesis route

The two inhibitors o-DPAPMP and m-DPAPMP (Fig. 1) were synthesised in the lab using a reported procedure[14]. 2-Pyridine formaldehyde (1 mmol) or 3-pyridine formaldehyde (1 mmol) was added to aniline (1 mmol) and triethyl phosphite (1 mmol) in the presence of solid $CoCl_2.6H_2O$ (1 mmol). After being heated to 373.15 K, the solution was refluxed for the proper amount of time. The progress of the reaction was observed using TLC (n-hexane/ethyl acetate). After extracting the reaction mixture, after being separated, the organic phase was dried over anhydrous $MgSO_4$. Filtrates were evaporated and recrystallized using ethanol before being dried at room temperature. The two molecular structures of the compounds were examined using melting point, FT-IR, UV–Vis, and NMR (^{1}H, ^{13}C, ^{31}P) spectroscopy (Supplementary Information).

Diethyl ((phenylamino) (pyridin-2-yl) methyl) phosphonate (o-DPAPMP): Brown solid: Yield 77%; melting point 110°C; UV–Vis (MeOH): λ_{max1} = 206.64 nm, λ_{max2} = 243.76 nm, λ_{max3} = 293.539 nm. IR (Solid state), ν (cm^{-1}): $\nu_{(N–H)}$ (3298), $\nu_{(C–H)\ aliphatic}$ (2853-3050), $\nu_{(C=C),}$ $\nu_{(C=N)\ aromatic}$ (1603-1500), $\nu_{(P=O)}$ (1235), $\nu_{(P-O),}$ $\nu_{(P–O\ –C)}$ (696-745). ^{1}H NMR (400 MHz, DMSO-d 6), δ (ppm): 1.162 (3H, t, J=7.1, -CH_2-C$\underline{H}_3$),1.271 (3H, t, J= 7.1, -CH_2-C$\underline{H}_3$), 3.901 - 4.149 (4H, m, -C$\underline{H}_2$- CH_3), 4.971 (1H, $\underline{H}$-C-P), 5.031 (1H, -N$\underline{H}$), 6,617 (1H,-C$\underline{H}_{Ar}$), 6.698 (2H, -C$\underline{H}_{Ar}$), 7.051(1H, -C$\underline{H}_{Ar}$), 7.122(1H, -C$\underline{H}_{Ar}$), 7.192 (1H,-C$\underline{H}_{Ar}$), 7.505(1H,-C$\underline{H}_{Ar}$), 7.641(1H,-C$\underline{H}_{Ar}$), 8.600 (1H, -C$\underline{H}_{Ar}$). ^{13}C NMR (400 MHz, DMSO-d 6):δ (ppm): 16.281 (1C, d, J=6.0, $\underline{C}H_3$-CH_2-), 16.456 (1C, d, J=6.0, $\underline{C}H_3$-CH_2-), 55.957-57.467 (2C, CH_3-$\underline{C}H_2$-), 63.688 (1C, H-$\underline{C}$-P), 114.036 (2C, -$\underline{C}H_{Ar}$), 118.410 (1C, -$\underline{C}H_{Ar}$), 123.565 (1C, -$\underline{C}H_{Ar}$), 123.740 (1C, -$\underline{C}H_{Ar}$), 129.412 (2C, -$\underline{C}H_{Ar}$), 137.775 (1C, - $\underline{C}H_{Ar}$), 146.830 (1C, -$\underline{C}H_{Ar}$), 148.944 (1C, -$\underline{C}H_{Ar}$), 156.176 (1C, -$\underline{C}H_{Ar}$). ^{31}P NMR (400 MHz, DMSO-d 6), δ (ppm): 21.452 (1P, -C-$\underline{P}$O (OC_2H_5)$_2$.

Diethyl ((phenylamino) (pyridin-3-yl) methyl) phosphonate (m-DPAPMP): Brown solid: Yield 75%; melting point 113°C; UV–Vis (MeOH): λ_{max1} = 206.520 nm, λ_{max2} = 230.804 nm, λ_{max3} = 259.184 nm. IR (Solid state), ν (cm^{-1}): $\nu_{(N–H)}$ (3308), $\nu_{(C–H)\ aliphatic}$

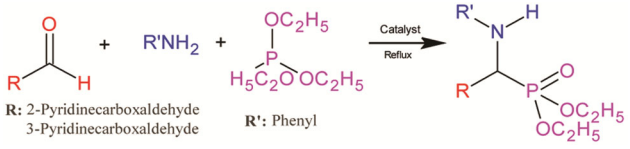

Fig. 1 — Synthesis of o-DPAPMP and m-DPAPMP

(2853- 3033), $\nu_{(C=C),\ \nu\ (C=N)\ aromatic}$ (1603-1509), $\nu_{(P=O)}$ (1236), $\nu_{(P-O),}\ \nu_{(P-O\ -C)}$ (692-754). ^{1}H NMR (400 MHz, DMSO-d 6),δ (ppm): 1.064 (3H, t, J=7.0, -CH_2-C$\underline{H}_3$), 1.188 (3H, t, J=7.0, -CH_2-C$\underline{H}_3$), 3.815-4.070 (4H, m, J=28.9, C$\underline{H}_2$-CH_3), 5.133 (1H, $\underline{H}$-C-P), 5.197 (1H, -N$\underline{H}$), 6.375 (1H, -C$\underline{H}_{Ar}$), 6.549 (1H, -C$\underline{H}_{Ar}$), 6.821 (2H, -C$\underline{H}_{Ar}$), 7.018 (1H, -C$\underline{H}_{Ar}$), 7.343(1H, -C$\underline{H}_{Ar}$), 7.906 3 (1H, -C$\underline{H}_{Ar}$) , 8.432(1H, -C$\underline{H}_{Ar}$), 8.716(1H, -C$\underline{H}_{Ar}$). ^{13}C NMR (400 MHz, DMSO-d 6), δ (ppm): 16.500 (1C, d, J=6.2 Hz,C$\underline{H}_3$-CH2-), 16.748 (1C, d, J=6.2,C$\underline{H}_3$-CH_2-), 51.328- 52.815 (2C, CH_3-C$\underline{H}_2$-), 63.022 (1C, H-C-P), 114.087 (2C, - C$\underline{H}_{Ar}$), 117.652 ppm (1C, - C$\underline{H}_{Ar}$), 123.681 (1C, - C$\underline{H}_{Ar}$), 129.142 (2C, - C$\underline{H}_{Ar}$), 133.276 (1C, - C$\underline{H}_{Ar}$), 136.083 (1C, - C$\underline{H}_{Ar}$), 147.369 (1C, - C$\underline{H}_{Ar}$), 148.915 (1C, - C$\underline{H}_{Ar}$), 150.147(1C, - C$\underline{H}_{Ar}$). ^{31}P NMR (400 MHz, DMSO-d 6), δ (ppm): 22.080 (1P, -C-PO $(OC_2H_5)_2$.

Experimental techniques

Weight loss experiments

For a 24 h immersion period at room temperature with aeration, all procedures were conducted in 50 mL of 0.5 M H_2SO_4 solution containing varying concentrations of α-aminophosphonate compounds. The cylindrical XC48 carbon steel samples were first abraded with abrasive paper, then thoroughly cleaned with distilled water, degreased with acetone, and finally dehydrated before each handling. After each test, the samples were cleaned with distilled water, dried, and weighed. The corrosion rate was calculated using the following equations[5-7].

$$W = \frac{W_1 - W_2}{S \times t} \quad \ldots (1)$$

Where: W_1 and W_2 are the mass of the specimen before and after corrosion, respectively, S stands for overall sample area, t for each experience's duration, and W for corrosion rate, the equation (2) was used to compute the inhibitory efficiency (IE %)

$$IE\ \% = \frac{W_0 - W_{inh}}{W_0} \times 100 \quad \ldots (2)$$

Where: W_0 and W_{inh} represent the corrosion rate without and with the inhibitor, respectively.

Electrochemical measurements

Electrochemical measurements were conducted in a conventional three-electrode glass cell, using a large grid platinum auxiliary electrode (CE) with an area of 2 cm^2, a calomel reference electrode (SCE), and an XC48 working electrode (WE) in the form of a disk with an exposed area of 0.2 cm^2 to the corrosive solution. Before use, the working electrode was abraded with various grades of abrasive paper, then cleaned with acetone and distilled water. The electrode was then immersed in the test solution at open circuit potential (OCP) for 30 min to achieve maximum stability. Electrochemical measurements were carried out using a PGZ 301 Volta Lab-40 model, and the data were analyzed with Volta Master IV software.

Polarization curves were obtained by automatically varying the electrode potential from -800 to -200 mV at as can rate of 0.5 mV/s. The corrosion current density (i_{corr}) and corrosion potential (E_{corr}) were determined, and the inhibition efficiency (IEp) was calculated using Eq. (3) based on the polarization curve data[5-7].

$$IEp\% = \left(\frac{i_{corr} - i^{\circ}_{corr}}{I_{corr}}\right) \times 100 \quad \ldots (3)$$

Where, i_{corr} and i°_{corr} represent the corrosion current density values with and without the inhibitors, respectively.

Electrochemical impedance spectroscopy (EIS) measurements were performed over a frequency range of 100 kHz to 10 MHz, with signal amplitude of 10 mV. The charge transfer resistance (Rct) was determined from the diameter of the semicircle in the Nyquist plot. The inhibition efficiency obtained from EIS was calculated using Eq. (4) [5-7].

$$IE_{EIS}(\%) = \frac{(R_{ct} - R^{\circ}_{ct})}{R_{ct}} \times 100 \quad \ldots (4)$$

Where, the charge transfer resistance values for steel with and without the inhibitors are denoted as R_{ct} and R°_{ct}, respectively.

Surface analysis

Atomic force microscopy

The surface images of the corroded samples, both with and without the addition of inhibitors, were obtained using atomic force microscopy (AFM). After immersion in a 0.5 M H_2SO_4 solution, with and without the addition of 10^{-3} M of o-DPAPMP or m-DPAPMP at 25°C for 24 h, the samples were washed with distilled water, dehydrated, and then examined using an MFP-3D Classic AFM system from Asylum Research and Oxford Instruments.

Contact angle measurements

Contact angle measurements were performed at room temperature after 24 h of immersion, with the

angles measured from droplet images using an optical goniometer equipped with Meter (Biolin Scientific) image capture software. Initially, a baseline test was conducted without corrosion inhibitors. Following this, the inhibitors were applied to the XC48 steel surface by placing a 3 to 5 µL drop of the selected solvent using a syringe. The drop was immediately observed after deposition and equilibration, and the device software automatically determined the contact angle.

Calculation method

Quantum chemical

The relationship between the inhibitive efficiency and the molecule's structure was explained using quantum chemical calculations. The Lee-Yang-Parr correlation functional (B3LYP) was applied with a basic 6-31G (d,p) set and Beck's three-parameters hybrid exchange functional[16]. Density Functional Theory (DFT) was used to optimize the geometry of ligands, and further optimization was carried out using the Gaussian 09 application package[17], with the results visualized through Gauss View 5.0.8 software[18]. Molecular orbital energies (HOMO and LUMO), dipole moment (µ), energy gap (ΔE_{gap}), global hardness (η), global softness (σ), absolute electronegativity (χ), electrophilicity index (ω), electron transfer (ΔN), and back-donation ($\Delta E_{Back\text{-}donation}$) of the molecules were all estimated using the following formulae[19, 20].

$$\Delta E_{gap} = E_{LUMO} - E_{HOMO} \quad \ldots(5)$$

$$\eta = \frac{E_{LUMO} - E_{HOMO}}{2} \quad \ldots(6)$$

$$\sigma = \frac{1}{\eta} \quad \ldots(7)$$

$$\chi = \frac{-(E_{HOMO} + E_{LUMO})}{2} \quad \ldots(8)$$

$$\omega = \left(\frac{\chi^2}{2\eta}\right) \quad \ldots(9)$$

$$\Delta N = \frac{\chi_{Fe} - \chi_{inh}}{2(\eta_{Fe} + \eta_{inh})} \quad \ldots(10)$$

$$\Delta E_{(Back-donation)} = \frac{\eta}{4} \quad \ldots(11)$$

Molecular dynamic simulations

Molecular dynamics (MD) simulations are commonly used to investigate the mechanism and configuration of inhibitor molecule adsorption on metal surfaces, as well as to calculate the adsorption and absorption interaction energies between inhibitors and iron[6,21]. The molecular dynamics simulations (MDS) were conducted using the Materials Studio 7.0 program[22]. A simulation box of dimensions 17.20 x 22.93 x 22.93 Å^3 was employed for the MD simulations. The Fe (110) crystal surface was chosen for this simulation, as it is the most stable surface reported in the literature[23]. Using the corrosion method, a blank plaque of 15 microns thickness was created after applying the α-aminophosphonates to the Fe surface. The MD simulations were carried out at 298 K, NVT, with a simulation time of 50 ps and a time step of 0.1 fs. The interaction energy ($E_{interaction}$) and binding energy ($E_{binding}$) of the inhibitor molecules on the Fe (110) surface were calculated using the equations 12 and 13[24].

$$E_{\text{interaction}} = E_{total} - E_{Fe+H2O} - E_{inhibitor} \quad \ldots(12)$$

$$E_{binding} = -E_{interaction} \quad \ldots(13)$$

Where: E_{total} is the system's total energy, E_{Fe+} is the energy of the iron surface in combination with H_2O molecules, $E_{inhibtor}$ is the energy of the inhibitor molecule alone, and the binding energy is the negative value of $E_{interaction}$.

Results and Discussion

Weight loss experiments

Table 1 and Fig. 2, combine weight loss values for carbon steel following 24 h of insertion in 0.5 M H_2SO_4 solutions with and without varying concentrations of the two inhibitors. The increasing inhibition efficiency with increasing concentration of the studied inhibitors indicates that these inhibitors protect the surface of the carbon steel where, the two inhibitors reach an inhibition rate of 94.56% and 93.66% at 10^{-3}M for o-DPAPMP and m-DPAPMP, respectively.

Table1 —Corrosion parameters of carbon steel X48 obtained from gravimetric measurements in 0.5 M H_2SO_4 solution containing various concentrations of o-DPAPMP and m-DPAPMP

Inhibitors	C_{inh} (M)	W (mg cm^{-2} h^{-1})	IE_W (%)
	Blank	2.4230	-
o-DPAPMP	10^{-6}	0.4157	82.84
	10^{-5}	0.2482	89.75
	10^{-4}	0.0934	93.17
	10^{-3}	0.0744	94.56
	10^{-6}	0.3700	84.72
m-DPAPMP	10^{-5}	0.2331	90.37
	10^{-4}	0.2031	91.61
	10^{-3}	0.1534	93.66

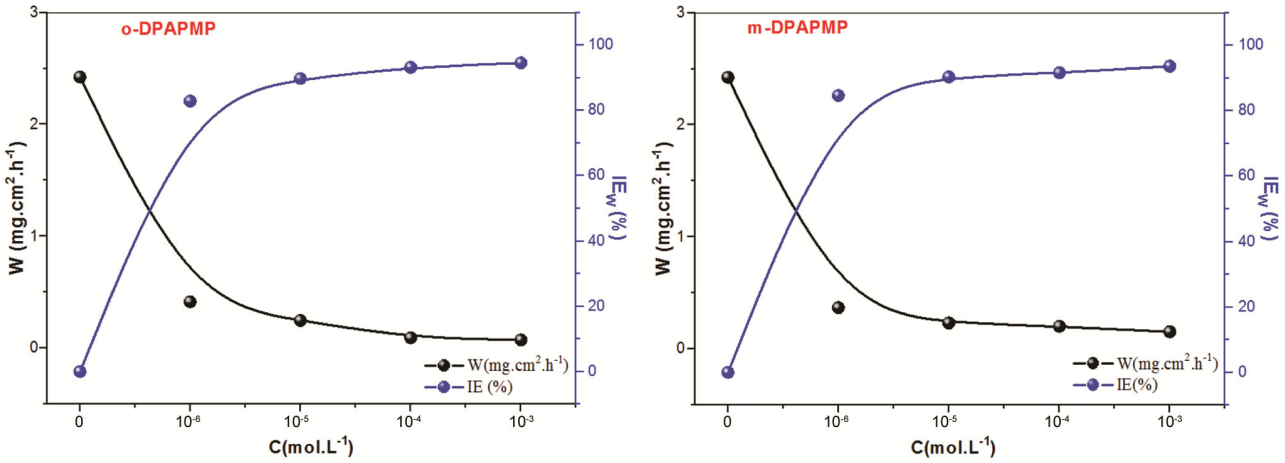

Fig. 2 — Relation between W and IE_W of carbon steel X48 electrode obtained in 0.5 M H_2SO_4 solution containing different concentrations of o-DPAPMP and m-DPAPMP

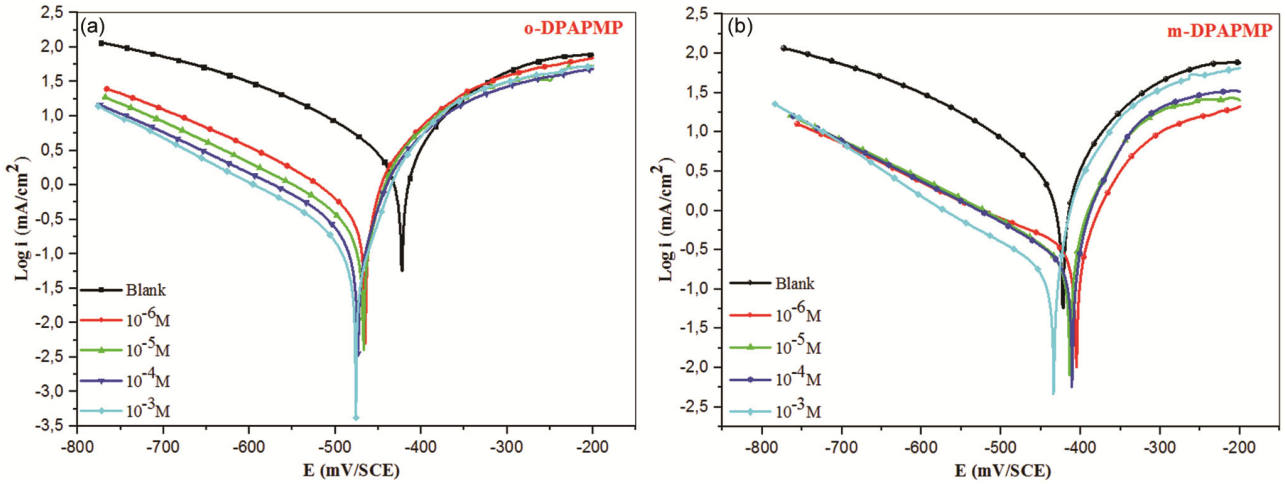

Fig. 3 — Polarization behaviour of carbon steel X48 in 0.5M H_2SO_4 solution containing different concentrations of o-DPAPMP and m-DPAPMP

Electrochemical measurements

Potentiodynamic polarization study

The polarization graphs of carbon steel XC48 immersed in 0.5 M H_2SO_4 solution containing various concentrations of α-aminophosphonates are shown in Fig. 3. The electrochemical parameters, including corrosion current densities (i_{corr}), corrosion potential (E_{corr}), cathodic Tafel slope (β_c), anodic Tafel slope (β_a) and inhibition efficiency (IE%) values, were calculated from the corresponding polarization curves, and are summarized in Table 2. An initial analysis of these curves reveals that both anodic and cathodic reactions are affected by the addition of inhibitors in 0.5 M H_2SO_4 solution, leading to a reduction in the following:

The anodic current associated with the metal dissolution process, represented by the reaction: $Fe \rightarrow Fe^{2+} + 2e^-$

The cathode current related to the proton reduction process:

$2H^+ + 2e^- \rightarrow H_2$

The results of Table 2 indicate that the investigated inhibitors act on both the cathodic and anodic processes, effectively reducing the corrosion of carbon steel, thus functioning as mixed-type inhibitors. The increase in inhibition efficiency with concentration suggests that these inhibitors protect the carbon steel surface, likely due to their adsorption onto the metal surface, forming a protective layer that shields it from corrosion[6,25]. This can be explained by the presence of N, O, and P atoms in the aminophosphonates structure, which form coordination bonds with free electron pairs and the d-orbitals of the iron surface, and the benzene ring is a excellent electron transporter[26]. Table 2 also, highlights that o-DPAPMP achieves the highest

Table 2 — Polarization parameters and corresponding inhibition efficiency for the carbon steel X48 in 0.5 M H_2SO_4 without and with addition of various concentrations of o-DPAPMP and m-DPAPMP compounds

Inhibitors	C_{inh}(M)	E_{corr} (mV/SCE)	i_{corr} (mA/cm^2)	β_a (mV/decade)	-β_c (mV/decade)	Rp (Ω.cm^2)	IE_P (%)
	Blank	-422.5	1.636	61.8	102.7	8.30	-
o-DPAPMP	10^{-6}	-468.1	0.3075	43.0	139.6	37.07	81.20
	10^{-5}	-467.3	0.1820	33.7	99.0	63.71	88.87
	10^{-4}	-473.7	0.1169	36.1	81.3	94.53	92.48
	10^{-3}	-475.9	0.0989	36.0	73.3	148.83	93.95
	10^{-6}	-405.0	0.2672	48.8	158.9	43.99	83.66
m-DPAPMP	10^{-5}	-410.7	0.2104	34.4	146.4	50.94	87.13
	10^{-4}	-413.8	0.1690	32.4	148.4	56.16	89.66
	10^{-3}	-434.0	0.1315	23.6	121.9	147.98	91.96

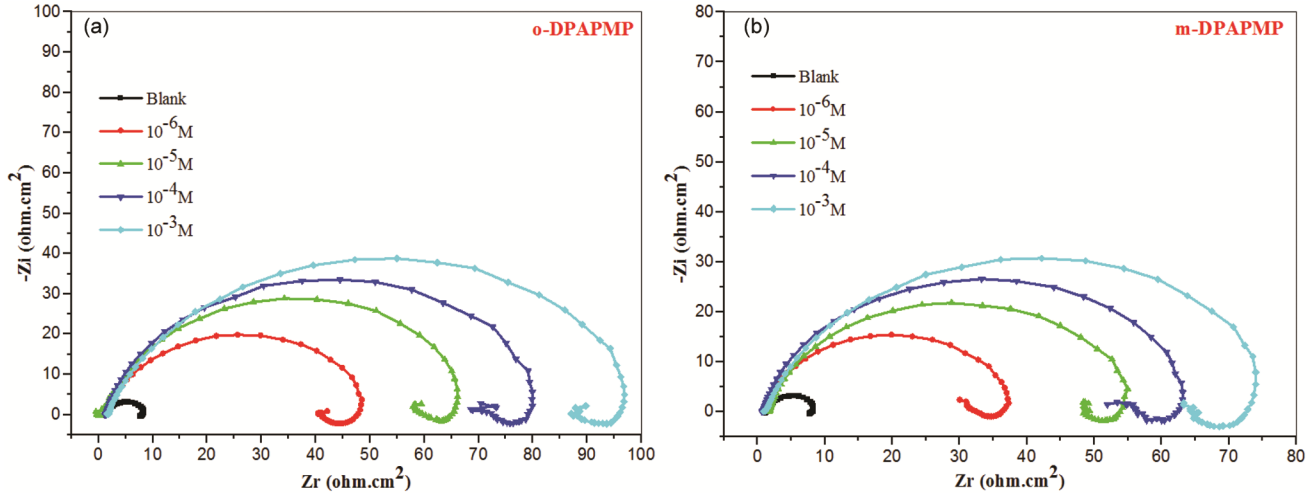

Fig. 4 — Nyquist plots for carbon steel X48 in 0.5 M H_2SO_4 solution containing different concentrations of α-aminophosphonates compounds at 25°C

inhibition efficiency value of 93.95%. This result can be attributed to the position of the N atom in the pyridine structure, which acts as an electron-donating group. Its location within thearomatic structure influences the molecule's capacity to inhibit[27,28].

Electrochemical impedance spectroscopy study (EIS)

The Nyquist plots of carbon steel in a 0.5 M H_2SO_4 solution, both with and without various concentrations of o-DPAPMP and m-DPAPMP are given in Fig. 4. The impedance parameters derived from these plots, including charge transfer resistance (R_t) and double-layer capacitance (C_{dl}) are given in Table 3. From the plots, it is evident that all impedance spectra exhibit a single capacitive loop, indicating that the corrosion of carbon steel in 0.5 M H_2SO_4 is mostly controlled by the charge transfer process, which is typically associated with double-layer behaviour[5,7,20]. All plots correspond to a depressed semi-circular shape at high frequencies and a small inductive loop at low frequencies[29]. The capacitive semi-circular loop at high-frequencies is attributed to the charge transfer resistance (R_{ct}), while the small inductive loop at low-frequencies may be attributed to the relaxation process of the adsorbed intermediates[29]. The increase in R_{ct} values is a result of inhibitor adsorption on metal surface, indicating a reduction in the exposed

Table 3 — Electrochemical impedance parameters for carbon steel X48 in 0.5 M H_2SO_4 without and with various concentrations of α-aminophosphonates compounds

Inhibitors	C_{inh}(M)	R_s (Ω.cm^2)	R_p (Ω.cm^2)	C_{dl} (μF. cm^{-2})	IE_{EIS} (%)
	Blank	1.126	7.802	322.2	-
o-DPAPMP	10^{-6}	2.958	31.93	124.5	75.56
	10^{-5}	3.603	44.85	88.69	82.60
	10^{-4}	2.278	76.76	65.51	89.83
	10^{-3}	1.434	80.43	49.45	90.29
	10^{-6}	0.989	37.24	72.18	79.04
m-DPAPMP	10^{-5}	1.681	55.11	67.52	85.84
	10^{-4}	1.288	63.89	64.56	87.88
	10^{-3}	0.882	77.88	62.27	89.98

surface area, likely due to the formation of a protective layer and increased surface coverage. While the decrease in C_{dl} values may be attributed to a reduction in local dielectric constant and/or an increase in courant density, suggesting that the inhibitors act by adsorbing onto the metal-solution interface[30]. Additionally, the diameters of the semi-circles in these plots depend on the concentration of the inhibitors, increasing as the concentration rises. This suggests that the exposed surface area of the metal increases with higher inhibitor concentrations, leading to increased the inhibition efficiency. These results correlate with the results obtained from weight loss and polarization measurements.

After examining the impedance plots, an equivalent electrical circuit was developed to model the behaviour of the metal/solution interface. The impedance plots were created using the ZSimpWin impedance fitting software for both the blank and inhibitor- containing solutions. The resulting circuit is shown in Fig. 5. This equivalent circuit consists of five components: a constant phase element (CPE), which replaces the double-layer capacitance (C_{dl}) to account for surface inhomogeneities[29,30]; R_s, representing the electrolyte resistance; R_{ct}, the charge transfer resistance; L, the inductance; and RL, the resistance of the inductor element.

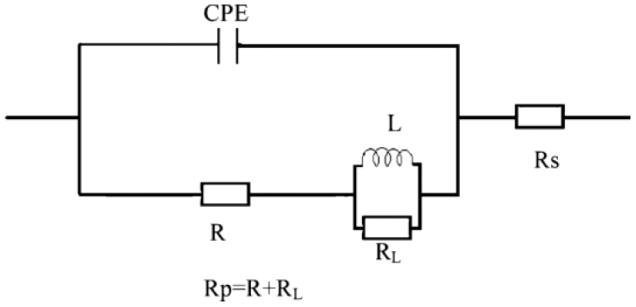

Fig. 5 — Equivalent circuit for XC48 carbon steel obtained under 0.5 M H_2SO_4

Numerous studies have demonstrated that heteroatom-containing compounds, such as α-aminophosphonates and organophosphorus compounds, possess inhibitory effects on the corrosion of carbon steel[30,31]. In Table 4, we compare o-DPAPMP and m-DPAPMP with other inhibitors and their corresponding efficiencies to evaluate their effectiveness as anticorrosion agents. As shown in Table 4, o-DPAPMP and m-DPAPMP, members of the α-aminophosphonates family, exhibit significant potential as novel inhibitors for carbon steel in acidic environments. These inhibitors are also anticipated to have a significant impact on the inhibition of other metals and under various conditions.

Adsorption isotherm

Calculating the adsorption isotherm is critical for understanding the corrosion inhibition process, as it characterizes the nature of the interaction between the inhibitor molecules and the metal surface. In this study, the Langmuir isotherm provides the best fit, and the following equation was used to describe it[32].

$$\frac{C_{inh}}{\theta} = \frac{1}{K_{ads}} + C_{inh} \quad \ldots (14)$$

Where: θ is the surface coverage, $\boldsymbol{C}_{inh}$ is the inhibitor concentration, K_{ads} is the equilibrium constant.

The adsorption constant values derived from the plots of C_{inh}/θ versus C_{inh}, plots (Fig. 6). The regression coefficient R^2 was found to be approximately 0.9999, indicating that the adsorption process of the o-DPAPMP and m-DPAPMP on the metal surface supports the validity of this model.

Additionally, the inhibition mechanism of the corrosion process can be deduced from the adsorption isotherm by estimating the standard Gibbs free energy ($\Delta G°_{ads}$) using the following equation[32].

$$K_{ads} = \frac{1}{55.5} \exp \frac{\left(-\Delta G^0_{ads}\right)}{RT} \quad \ldots (15)$$

Table 4 —Comparison of corrosion inhibition efficiency of o-DPAPMP and m-DPAPMP with the literature data on XC48 carbon steel under acidic environments

	Inhibition efficiecy at optical concentration in acidic medium			
Reference	Djenane et al.[30]	Moumeni et al.[31]	o-DPAPMP	m-DPAPMP
Structure	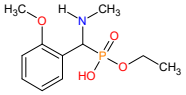	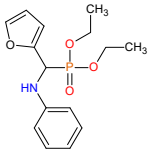	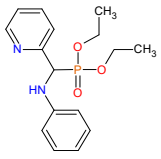	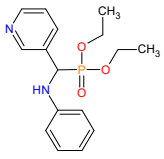
E_{PDP} (%)	89.16	63.82	93.95	91.96
E_{EIS} (%)	81.91	83.34	90.29	89.98

Where: 55.5 is the molar concentration of water in the solution expressed in mol/L, R is the gas constant (8.314 J/K mol), T is the absolute temperature (K).

It has been reported that energy-free standard values of -20 kJ/mol or less are associated with electrostatic interaction between charged molecules and metals, indicating physisorption as the adsorption mechanism. In contrast, values greater than -40 kJ/mol suggest chemisorption, implying coordination with a metal band[5, 25]. According to previous studies, a high value of the adsorption equilibrium constant (K_{ads}) indicates that the inhibitors are more readily and effectively adsorbed onto the metal surface[5,7,25]. In this investigation, both inhibitory showed K_{ads} values in the range of 10^5, providing superior inhibition performance of these α-aminophosphonates compounds. As shown in Table 5, the calculated standard Gibbs free energies for the investigated inhibitors, o-DPAPMP and m-DPAPMP, range from -37 to -38 kJ/mol is suggesting both physical and chemical adsorption[33]. These values also indicated that the inhibitors are strongly bonded to the metal surface.

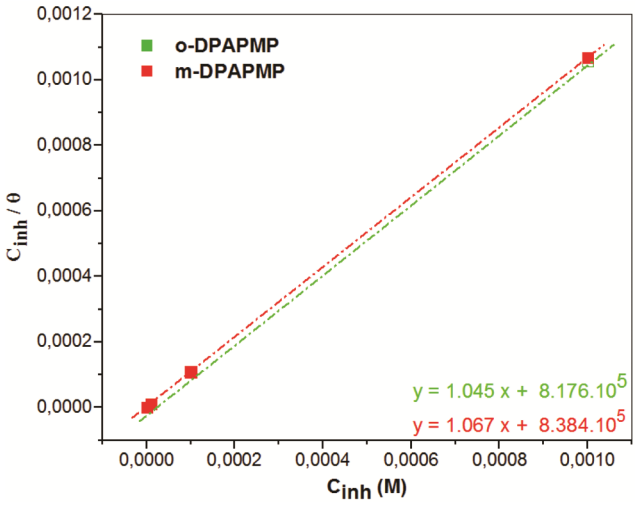

Fig. 6 —Langmuir adsorption plots for carbon steel X48 in H_2SO_4 M containing different concentrations of o-DPAPMP and m-DPAPMP

Surface analytical AFM analyses

AFM analyses

Atomic force microscopy (AFM) is gaining recognition as an effective tool for investigating the corrosion process at the metal/solution interface, as it allows for detailed examination of surface morphology at both microscopic and nanoscale levels[34]. Fig. 7 displays both two-dimensional and three-dimensional AFM images of the carbon steel X48 surface before and after 24 h of immersion in a solution of 0,5 M H_2S0_4 with and without the presence of o-DPAPMP and m-DPAPMP. Table 6 summarizes the roughness values. The average roughness before and after immersion in the 0.5 M H_2S0_4 solution were found to be 15.600 nm and 134.278 nm, respectively (Figs 7a & 7b). In contrast, in the presence of 10^{-3} M of o-DPAPMP and m-DPAPMP, the roughness values were 100.757 nm and 103.395 nm respectively (Figs 7c & 7d). The reduced roughness values observed in the presence o-DPAPMP and m-DPAPMP, particularly when compared to the roughness after immersion in the acid solution without the inhibitors, suggest that these compounds are effective in reducing the corrosion rate and minimizing surface metal deterioration.

Contact angle measurements

The hydrophobic or hydrophilic characteristics of the surface, both in the presence and absence of inhibitors, can be easily detected by measuring the water contact angle. A contact angle greater than 90° indicates water-repellent properties, while an angle less than 90° signifies typical wetting behaviour[35]. For a freshly polished XC48 carbon steel surface, the contact angle is 69.60°. However, when the surface is immersed in a 0.5 M H_2SO_4 solution for 24 h, the contact angle raised to 42.14° (Fig. 8a and 8b). In contrast, when the surface is exposed to the highest concentration of inhibitor molecules in the H_2SO_4 solution, the contact angles increase. In presence of 10^{-3} M concentrations of o-DPAPMP and m-DPAPMP inhibitors, the contact angles raised to

Table 5 — Thermodynamic parameters of the adsorption of o-DPAPMP and m-DPAPMP on XC48 surface

Inhibitors	Methods	Slope	R^2	K_{ads} (M^{-1})	$\Delta G°_{ads}$ ($kJ.mol^{-1}$)
o-DPAPMP	Gravimetric	1.0450	0.99991	$8.1766.10^5$	-37.9570
	Polarization	1.0542	0.99998	$6.7267.10^5$	-37.4745
	Impedance	1.0884	0.99988	$5.6983.10^5$	-37.0647
m-DPAPMP	Gravimetric	1.0675	0.99999	$8.3843.10^5$	-38.0200
	Polarization	1.0864	0.99999	$8.7634.10^5$	-38.1296
	Impedance	1.1104	0.99999	$9.1157.10^5$	-38.2271

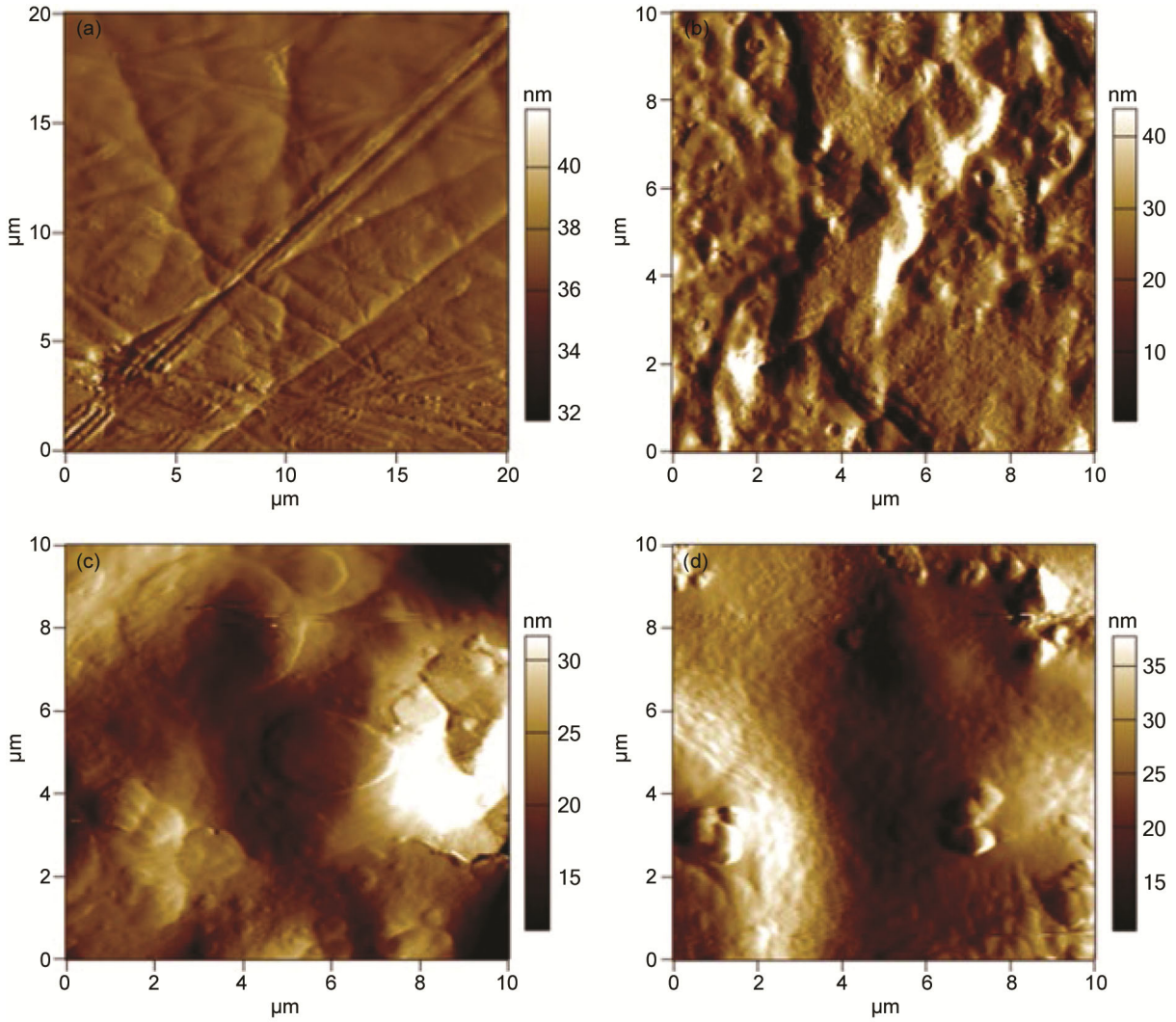

Fig. 7 — AFM image in 2D for inhibitors, after immersion in 0.5 M H_2SO_4 of carbon steel surface (a) Polished carbon steel, (b) Carbon steel in 0.5 M H_2SO_4, (c) with 10^{-3} M of o-DPAPMP and (d) with 10^{-3}M of m-DPAPMP

Table 6 —Roughness values of the XC48 steel obtained from AFM measurements in 0.5 M H_2SO_4 solutions with and without investigated inhibitors

AFM data	Polished XC48	Blank 0.5 M H_2SO_4	10^{-3} M Inhibitor	
Roughness (nm)	15.600	134.278	100.758[a]	103.395[b]

[a]o-DPAPMP and [b]m-DPAPMP

63.98° and 60.64°, respectively (Figs 8c and 8d). These results suggest that a water-repellent film forms on the steel surface in the presence of the inhibitor molecules. Moreover, the study reveals that the surface treated with o-DPAPMP exhibits better water-repellent propertiescompared to the surface treated withm-DPAPMP.

Quantum chemical parameters

To investigate the relationship between the molecular structures of these compounds and their inhibitory effectiveness, various quantum chemical simulations were performed. Fig. 9 shows the optimized molecular structures of the compounds, while Table 7 presents the key quantum chemical parameters that were evaluated.

The terms HOMO (Highest Occupied Molecular Orbital) and LUMO (Lowest Unoccupied Molecular Orbital) are key indicators of chemical reactivity, representing the ability of a molecule to donate and accept electrons, respectively. A low E_{LUMO} value indicates the molecule's ability to accept electrons, while a high E_{HOMO} value suggests better inhibitory action and enhanced adsorption of the inhibitor on the

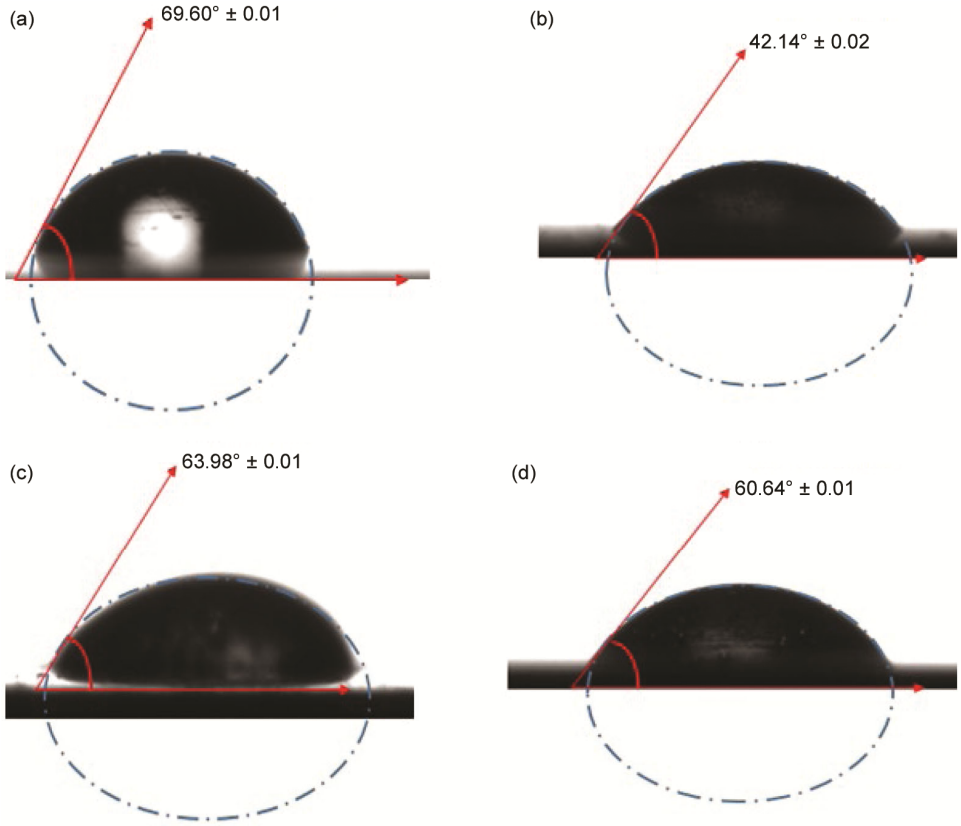

Fig. 8 — Contact angles measurements (a) on water (b) on polished carbon XC48 surface immersed in 0.5 M H_2SO_4 solution for 24 h with no inhibitor, (c) with 10^{-3} M of inhibitor o-DPAPMP and (d) with 10^{-3} M of inhibitor m-DPAPMP

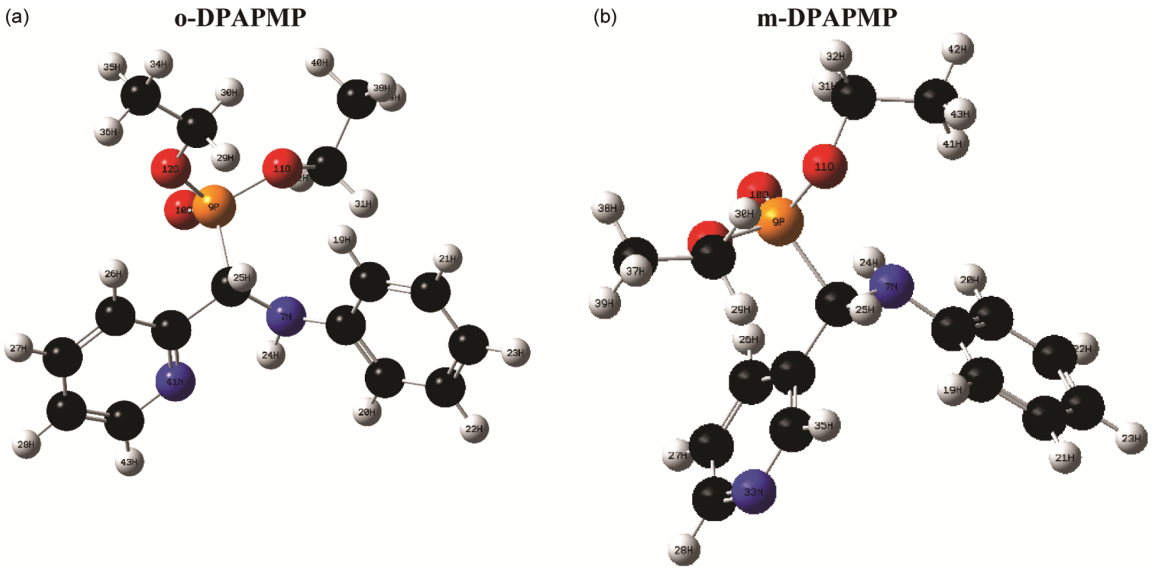

Fig. 9 — Optimized structures of o-DPAPMP and m-DPAPMP

metal surface[7, 35]. As the HOMO energy increases and the LUMO energy decreases, the inhibitor's ability to bind to the metal surface strengthens. With rising HOMO and falling LUMO energy values, the inhibitor's ability to attach to the metal surface increases. Fig. 10 shows the molecular orbital diagrams of o-DPAPMP and m-DPAPMP. For o-DPAPMP and m-DPAPMP, the respective E_{HOMO} values are -5.461 and -5.572 eV, while the corresponding E_{LUMO} values are -0.828 and -0.697 eV.

Table 7 — Quantum chemical parameters of o-DPAPMP and m-DPAPMP

Quantum chemical parameters	o-DPAPMP	m-DPAPMP
E_{HOMO} (eV)	-5.282	-5.449
E_{LUMO} (eV)	-0.842	-0.828
ΔE_{gap}(E_{LUMO}-E_{HOMO}) (eV)	4.440	4.621
E_{tot} (eV)	-35346.683	-35346.547
μ (debye)	3.348	2.122
η(eV)	2.220	2.310
σ(eV)	0.450	0.432
χ(eV)	3.062	3.138
ω(eV)	2.111	2.131
ΔN(eV)	0.886	0.835
$\Delta E_{(Back-donation)}$ (eV)	0.555	0.577

The higher E_{HOMO} value and lower E_{LUMO} value of o-DPAPMP indicate its superior inhibition efficiency. Furthermore, the energy gap (ΔE_{gap}) is another important parameter for assessing the inhibitor molecule's reactivity towards the metal surface. Lower ΔE_{gap} values correlate with better inhibition efficiency, as they reduce the energy required to remove an electron from the last occupied orbital[5, 35]. In this investigation, ΔE_{gap} follows the order o-DPAPMP < m-DPAPMP, suggesting that o-DPAPMP exhibits higher reactivity and is likely to interact more strongly with the metal surface.

Additionally, the molecular electrostatic potential (MEP) profile of a molecule provides a visual

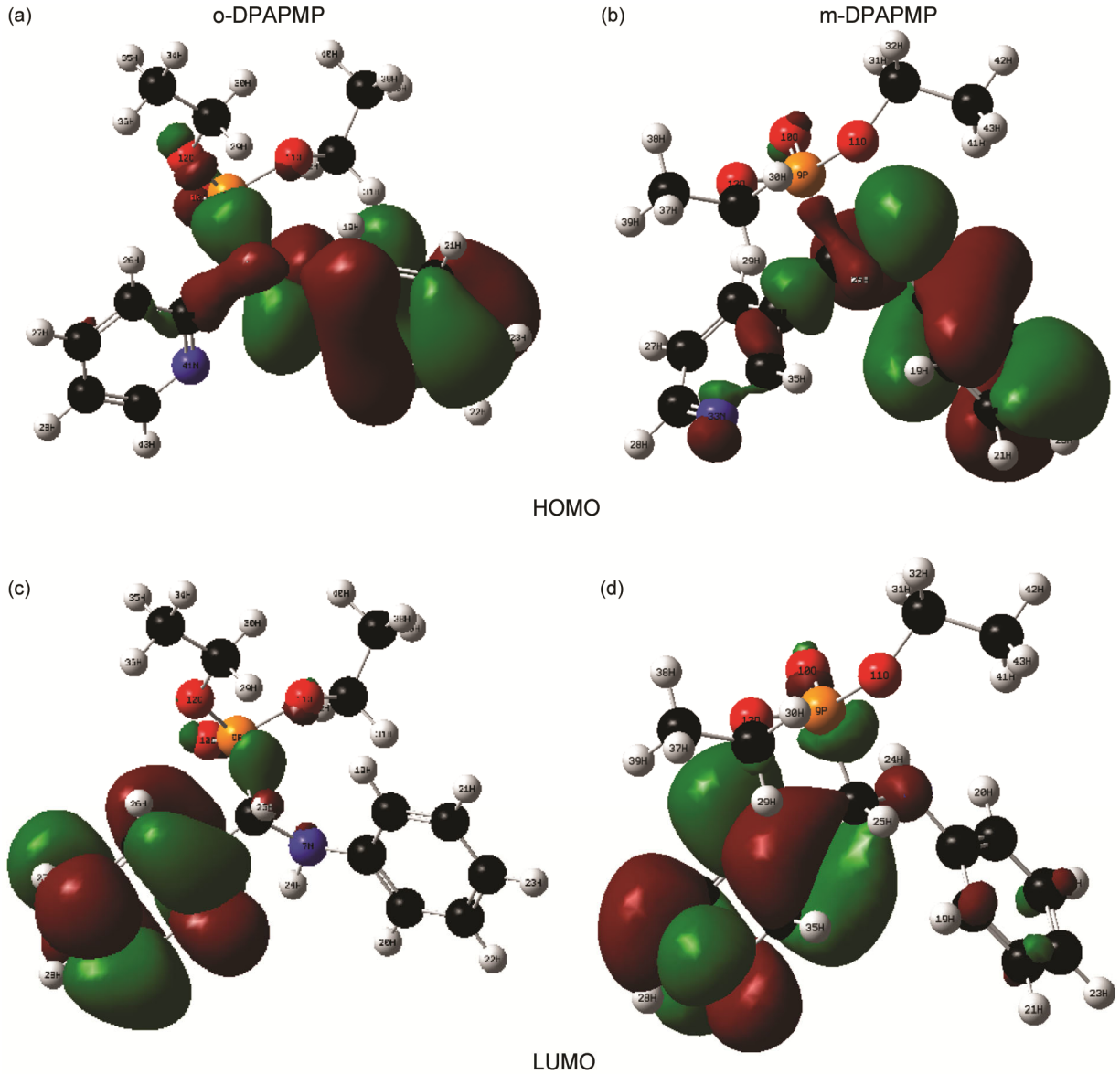

Fig. 10 — Representation of HOMO, LUMO densities of (a, c) o-DPAPMP and (b, d) m-DPAPMP

representation for identification of the binding sites and the interactions between the molecules and approaching species. The MEP's colour gradients reflect the electrostatic potential at the molecule's surface, with red regions indicating areas of attractive potential (nucleophilic reactivity) and blue regions indicating areas of repulsive potential (electrophilic reactivity)[36]. In the MEP map of the studied inhibitors (Fig. 11), negative potential zones correspond to the electronegative atoms (such the oxygen atoms of the phosphonate group), while, positive potential regions are associated with electropositive atoms (like hydrogen atoms). The MEP values for o-DPAPMP are $-6.917e^{-2}$ a.u. and $6.917e^{-2}$ a.u and for m-DPAPMP are $-5.668e^{-2}$ a.u. and $5.668e^{-2}$ a.u, respectively, suggesting significant potential for both electrophilic and nucleophilic attack. The predominantly green regions in the MEP surfaces represent areas of intermediate potential, positioned between the extremes of red and blue. A proton is attracted to molecules with concentrated electron density (from lone pairs, pi-bonds, etc.) when the electrostatic potential is negative. Conversely, in areas with low electron density and insufficient nuclear charge shielding, the positive electrostatic potential is associated with the repulsion of protons from the atomic nuclei[35,36]. The presence of both highly electronegative and electropositive regions, along with moderate sections in synthesized compounds, indicates the potential for strong electrophilic and

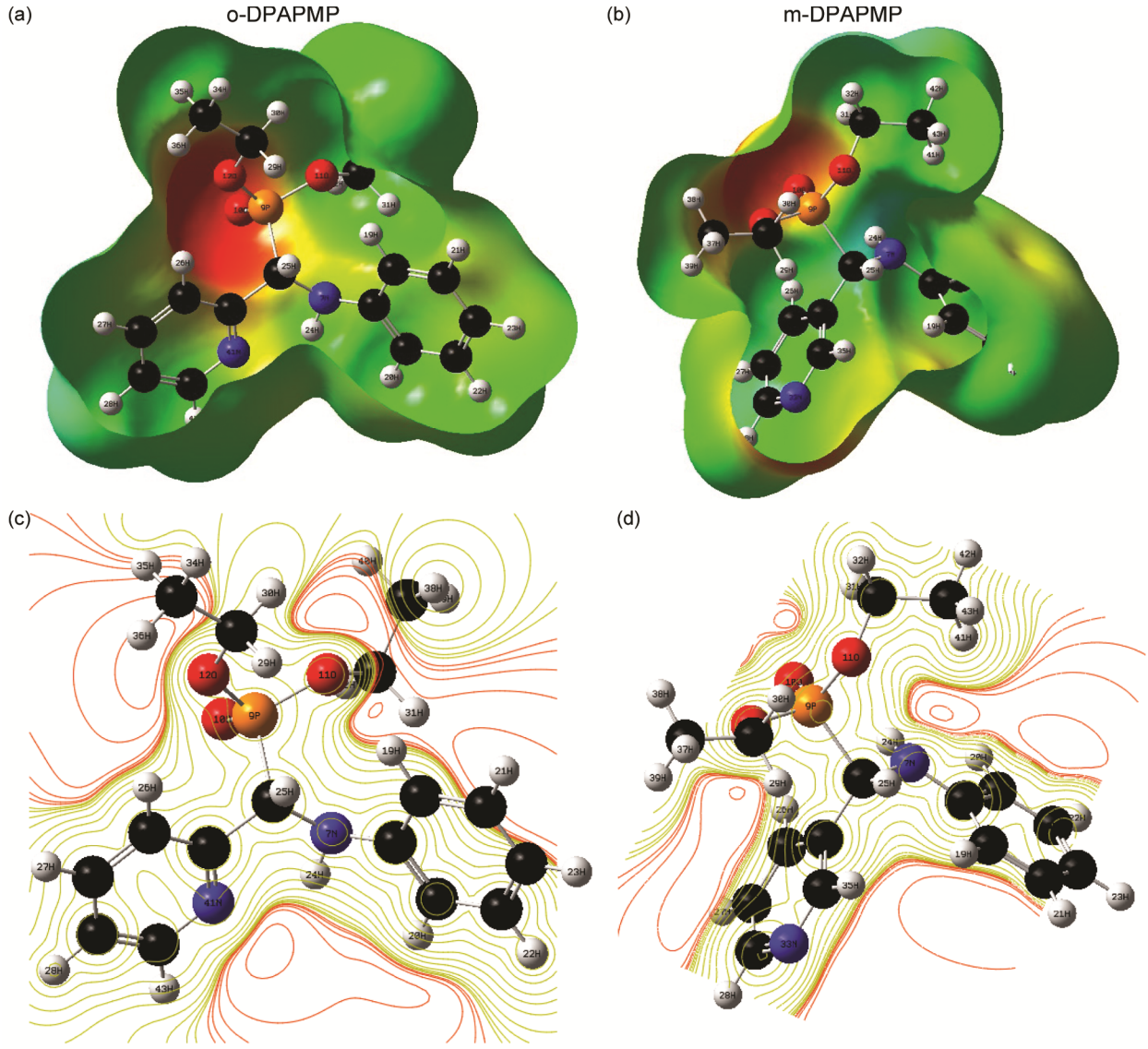

Fig. 11 — MEP maps in 3D and 2D of (a, c) o-DPAPMP and (b, d) m-DPAPMP

nucleophilic attack. The distribution of electrical density across the molecules offers insight into the likely adsorption sites on the metal surface, such as horizontal or parallel orientations.

The dipole moment can be used to forecast the overall surface coverage of aminophosphonates on an iron surface. Molecules possessing a significant dipole moment are expected to exhibit greater surface coverage when adsorbed onto the metal surface[20,32]. The results indicate that o-DPAPMP has the highest dipole moment (3.348 D), suggesting that it will adhere more strongly to the metal surface compared to m-DPAPMP and will therefore exhibit the highest inhibitory efficacy. Hardness and softness are significant variables that affect a molecule's molecular stability and reactivity. Higher inhibitory effectiveness is generally associated with higher and lower hardness values[6,7]. A soft molecule has a smaller energy gap compared to the largerenergy gap of a hard molecule[20,36]. In this investigation, the o-DPAPMP compound demonstrates the highest inhibitory efficiency, with a low hardness value of 2.316 eV and a high softness value of 0.431 eV, in comparison to the m-DPAPMP compound. The absolute electronegativity indicates a molecule's ability to attract electrons into covalent bonds. Molecules with low electronegativity values tend to reach electronic equilibrium more easily, resulting in increased reactivity. Conversely, a high electronegativity value demonstrates an inverse relationship[5,36]. Table 8 shows that the differential electronegativity changes between the inhibitor and metal follow the order o-DPAPMP < m-DPAPMP. These findings indicate that o-DPAPMP has the lowest electronegativity (3.062 eV) compared to m-DPAPMP, suggesting a higher inhibitory effectiveness. The electrophilicity index measures a molecule's capacity to accept electrons a high value of ω indicate a strong electron-accepting capacity of the molecule[36,37]. According to the experimental data, the electrophilicity values follow the order: o-DPAPMP > m-DPAPMP, which aligns with experimental observations. The ΔN depicts the trend of electron donation within a group of inhibitors. To determine the percentage of transferred electrons, the theoretical parameters χFe = 7.0 eV and ηFe = 0[(Ref. 6,25)] were applied. Furthermore, the ΔN values were computed and indicate that the inhibition efficiency due to electron donation agrees with the findings of Lukovits's study[20,37]. When ΔN < 3.6, the inhibition efficiency increases as the electron-donating ability of the inhibitors enhances their ability to donate electrons to the metal surface. The efficiency increases in the following order: o-DPAPMP > m-DPAPMP. These findings demonstrate that ΔN is strongly.

Table 8 — Interactions and binding energies estimated by MD simulations for the molecules adsorption on Fe (110) (in kJ mol^{-1})

Energies	o-DPAPMP	m-DPAPMP
Total energy	-91.49	-90.93
Adsorption energy	-158.16	-156.27
Rigid adsorption energy	-168.78	-165.12
Deformation energy	10.62	8.84
dE_{ad}/d_{Ni}	-158.16	-156.27

Back donation ($\Delta E_{Back\text{-}donation}$)

Gomez et al.[38] recently suggested that the interaction between the inhibitor molecule and the metal surface may be influenced by an electronic back-donation process, based on the charge transfer model for electron donation and back-donation. According to this model, when both the transfer of electrons to the molecule and back donation from the molecule occur simultaneously, the energy change is directly related to the molecule's hardness. The transfer of charge to the molecule, followed by back-donation from the molecule to the metal, is energetically favoured when η>0 and $\Delta E_{b\text{-}d} < 0$. The calculated $\Delta E_{b\text{-}d}$ values show the trend: o-DPAPMP < m-DPAPMP, indicating that o-DPAPMP exhibits the lowest back-donation level of back donation and the highest inhibitory efficiency, as expected and consistent with the experimental findings.

Molecular dynamic simulations

The standard charge molecular dynamics simulation is essential for understanding of the inhibitors' adsorption inhibitory on the surface of carbon steel. After optimization, MD simulations were used to estimate the adsorption energies of o-DPAPMP and m-DPAPMP on the Fe (110) surface. The corresponding adsorption geometries are shown in Fig. 12 and Table 8 correlated with the experimental inhibition efficiencies.

As shown in Fig. 12, the examined inhibitors are strongly bound to the iron atoms and adsorb onto the Fe (110) surface in a nearly horizontal orientation, with their hard inhibitor molecule structures aligning with the metal. Furthermore, an analysis of the inhibitor molecules reveals that, upon adsorption onto the metal surface, chemical interactions lead to the

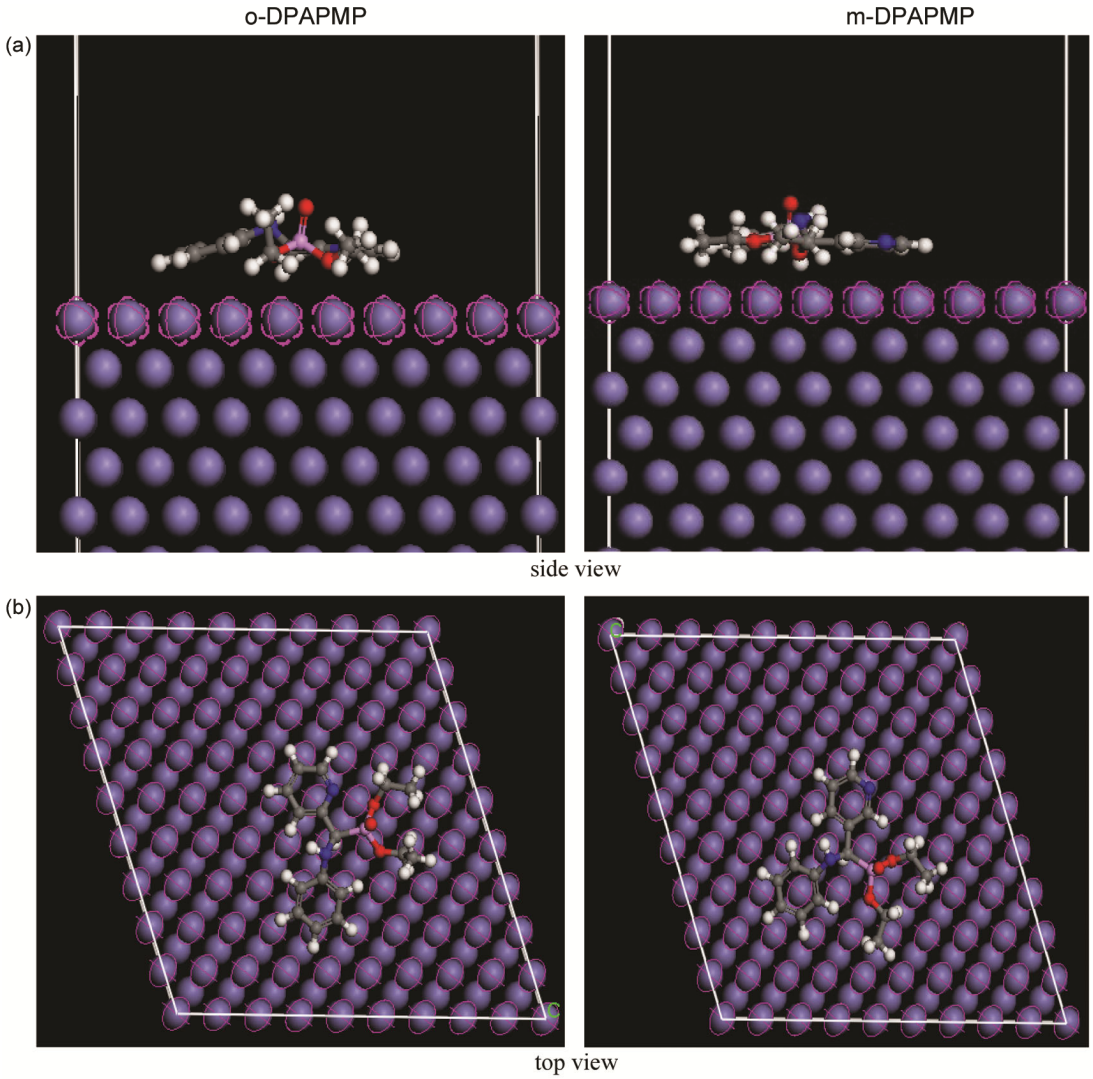

Fig. 12 — Equilibrium configurations of o-DPAPMP and m-DPAPMP on Fe(110) surface in vacuum slabs: (a) top view and (b) side view

transfer of the electrons from the nitrogen, oxygen, and aromatic rings of the inhibitors to iron atoms, forming coordinating bonds. The strength of atoms, forming physical interactions generally increases with the size of the molecule, and the physical connection between the inhibitor molecules and the metal surface, driven by van der Waals dispersion forces, may also influence the overall attraction overall the molecules and the surface[35,39]. The calculated interaction energies for the adsorption of o-DPAPMP and m-DPAPMP are -158.16 and -156.27 kJ mol^{-1}, respectively. The negative and relatively high values of these interaction energies indicate the strong adsorption of the inhibitor molecules onto the Fe surface[35,40]. As shown in Table 8,

Table 9 — The measured bond distances between the active centres of the inhibitors and Fe atoms

Inhibitors	o-DPAPMP	m-DPAPMP
Distances	$d_{Fe–O11}$=4.681A°	$d_{Fe–O11}$=4.716A°
	$d_{Fe–O10}$=3.540A°	$d_{Fe–O10}$=3.455A°
	$d_{Fe–O12}$=2.403A°	$d_{Fe–O12}$=2.959A°
	$d_{Fe–N41}$= 4.335A°	$d_{Fe–N41}$=4.360A°
	$d_{Fe–N7}$=3.062A°	$d_{Fe–N7}$=3.106A°

the binding energy follows the order o-DPAPMP> m-DPAPMP, indicating that o-DPAPMP has a better capacity for adsorption on the Fe surface. These results align with previous findings from experimental measurements and quantum mechanical calculations.

Additionally, Table 9 and Fig. S1 (Supplementary Information) display the observed equilibrium bond

lengths between the nearest heteroatoms of the inhibitor molecules and the Fe (110) surface. The significant inhibitory efficiencies were confirmed by the identification of chemical bonds forming between the active centres O10, O11, O12, N41, and N7 of the studied compounds and the Fe (110) atoms.

Conclusion

Both ortho and meta diethyl [(phenylamino) (pyridinyl) methyl] phosphonates, o-DPAPMP and m-DPAPMP, were synthesized via the Kabachnik-Fields reaction, with their structures confirmed using melting point, FT-IR, UV–Vis, and ^{1}H, ^{13}C, and ^{31}P nuclear magnetic resonance spectroscopy. The investigated compounds inhibit strong corrosion inhibition of carbon steel XC48 in a 0.5 M H_2SO_4 solution. As the concentrations of the inhibitors increases, so does the inhibition efficiency. Both inhibitors effectively reduce corrosion of the carbon steel XC48 in 0.5 M H_2SO_4, with gravimetric, polarization, and EIS measurements showing o-DPAPMP performing better than m-DPAPMP. The adsorption of both compounds follows the Langmuir's isotherm model, indicating they act as mixed-type corrosion inhibitors. The $\Delta G°_{ads}$ values further suggest both physical and chemical adsorption mechanisms. AFM analysis of the carbon steel XC48 surface reveals the formation of a stable, insoluble protective layer. Contact angle measurements indicate the development a water-repellent coating on the carbon steel surface in the presence of both inhibitors. Overall, the experimental results align closely with the theoretical values derived from quantum chemical calculations. Additionally, molecular dynamics simulations show that the two molecules adhere to the iron surface in a closely aligned, parallel orientation.

Acknowledgments

This research was supported by Algerian Ministry of Scientific Research, Laboratory of Electrochemistry of Molecular Materials and Complex (LEMMC), Ferhat ABBAS University of Setif.

Supplementary Information

Supplementary information is available on the website http://nopr.niscpr.res.in/handle/123456789.

Conflict of interest

The authors declare no conflict of interest.

References

1 Qiang Y, Zhang S, Xu S, Guo L, Chen X & Obot I B, Effective protection for copper corrosion by two thiazole derivatives in neutral chloride media: Experimental and computational study, *Int J Electrochem Sci*, 11 (2016) 3147.

2 Ech-chihbi E, Adardour M, Ettahiri W, Salim R, Ouakki M, Galai M, Baouid A & Taleb M, Surface interactions and improved corrosion resistance of mild steel by addition of new triazolyl-benzimidazolone derivatives in acidic environment, *J Mol Liq*, 387 (2023) 122652.

3 Zhipei C, Koleva D & van-Breugel K, A review on stray current-induced steel corrosion in infrastructure, *Corros Rev*, 35 (2017) 397.

4 Ferreira E S, Giacomelli C, Giacomelli F C & Spinelli A, Evaluation of the inhibitor effect of L-ascorbic acid on the corrosion of mild steel, *Mater Chem Phys*, 83 (2004) 129.

5 Mammeri S, Chafai N, Harkat H, Kerkour R & Chafaa S, Protection of steel against corrosion in acid medium using dihydropyrimidinone derivatives: Experimental and DFT study, *Iran J Sci Technol Trans A: Sci*, 45 (2021) 1607.

6 Kerkour R, Chafaa S, Maouche N, Moumeni O & Chafai N, Corrosion inhibition of stainless steel N_30_4 by dihydroxy benzyl phosphonic acid in 0.5 M H_2SO_4: Experimental and theoretical studies, 26 (2019) 69.

7 Moumeni O, Chafaa S, Kerkour R, Benbouguerra K & Chafai N, Synthesis, structural and anticorrosion properties of diethyl (phenylamino) methyl) phosphonate derivatives: Experimental and theoretical study, *J Mol Struct*, 1206 (2020) 127693.

8 Jaworska J, Genderen-Takken H V, Hanstveit A, van de Plassche E & Feijtel T, Environmental risk assessment of phosphonates, used in domestic laundry and cleaning agents in the Netherlands, *Chemosphere*, 47 (2002) 655.

9 Gledhill W E & Feijtel T C J, Environmental properties and safety assessment of organic phosphonates used for detergent and water treatment applications, *Detergents*, (1992) 261.

10 Kleszczynska H & Sarapuk J, New aminophosphonates with antioxidative activity, *Cell Mol Biol Lett*, 6 (2001) 83.

11 Zhao G, Lin H, Yu P, Sun H, Zhu S, Su X & Chen Y, Ethylenediamine-palladium (II) complexes with pyridine and its derivatives: Synthesis, molecular structure and initial antitumor studies, *J Inorg Biochem*, 73 (1999) 145.

12 Chafai N, Chafaa S, Benbouguerra K, Daoud D, Hellal A & Mehri M, Synthesis, characterization and the inhibition activity of a new α-aminophosphonic derivative on the corrosion of XC48 carbon steel in 0.5 M H_2SO_4: Experimental and theoretical studies, *J Taiwan Inst Chem Eng*, 70 (2017) 331.

13 Kabachnik M I & Medved T Y, New method for the synthesis of 1-aminoalkylphosphonic acids communication 1, *Bull Acad Sci USSR: Div Chem Sci*, 2 (1953) 769.

14 Karimi-Jaberi Z, Zare H, Amiri M & Sadeghi N, Cobalt (II) chloride accelerated one-pot three-component synthesis of α-aminophosphonates at room temperature, *Chin Chem Lett*, 22 (2011) 559.

15 Shokry H, Molecular dynamics simulation and quantum chemical calculations for the adsorption of some Azo-azomethine derivatives on mild steel, *J Mol Struct*, 1060 (2014) 80.

16 Becke A D, Density-functional thermochemistry. I. The effect of the exchange-only gradient correction, *J Chem Phys*, 96 (1992) 2155.
17 Frisch M J, Trucks G W, Schlegel H B, Scuseria G E, Robb M A, Cheeseman J R, Scalmani G, Barone V, Mennucci B, Petersson G A, Nakatsuji H, Caricato M, Li X, Hratchian H P, Izmaylov A F, Bloino J, Zheng G, Sonnenberg J L, Hada M, Ehara M, Toyota K, Fukuda R, Hasegawa J, Ishida M, Nakajima T, Honda Y, Kitao O, Nakai H, Vreven T, Montgomery J A, Peralta J E, Ogliaro F, Bearpark M, Heyd J J, Brothers E, Kudin K N, Staroverov V N, Kobayashi R, Normand J, Raghavachari K, Rendell A, Burant J C, Iyengar S S, Tomasi J, Cossi M, Rega N, Millam J M, Klene M, Knox J E, Cross J B, Bakken V, Adamo C, Jaramillo J, Gomperts R, Stratmann R E, Yazyev O, Austin A J, Cammi R, Pomelli C, Ochterski J W, Martin R L, Morokuma K, Zakrzewski V G, Voth G A, Salvador P, Dannenberg J J, Dapprich S, Daniels A D, Farkas O, Foresman J B, Ortiz J V, Cioslowski J & Fox D J, Gaussian 09, Revision A.02, Gaussian, Inc., Wallingford, CT, (2009).
18 Roy D, Keith T & Millam J, *Gauss View*, (2009).
19 Kohn W & Sham L J, Quantum density oscillations in an inhomogeneous electron gas, *Phys Review*, 137 (1965) A1697.
20 Benbouguerra K, Chafaa S, Chafai N, Mehri M, Moumeni O & Hellal A, Synthesis, spectroscopic characterization and a comparative study of the corrosion inhibitive efficiency of anα-aminophosphonate and Schiff base derivatives: Experimental and theoretical investigations, *J Mol Struct*, 1157 (2018) 165.
21 Kaya S, Lei G, Kaya C, Tüzün B, Obot I B, Touir R & Islam N, Quantum chemical and molecular dynamic simulation studies for the prediction of inhibition efficiencies of some piperidine derivatives on the corrosion of iron, *J Taiwan Inst Chem Eng*, 65 (2016) 522.
22 Materials studio, 7.0 San Diego, CA: Accelrys Inc.; (2013).
23 Guo L, Zhu S, Zhang S, He Q & Li W, Theoretical studies of three triazole derivatives as corrosion inhibitors for mild steel in acidic medium, *Corros Sci*, 87 (2014) 366.
24 Akkermans R L C, Spenley N A & Robertson S H, Monte Carlo methods in materials studio, *Mol Simul*, 39 (2013) 1153.
25 Kerkour R, Moumeni O, Djenane M, Chafai N & Chafaa S, Synergistic corrosion inhibitor of carbon steel by dihydroxy benzyl phosphonic acid-Zn^{2+} system in 0.5 M H_2SO_4: Experimental and theoretical studies, *Indian J Chem Technol*, 29 (2022) 402.
26 Meng Y, Ning W, Xu B, Yang W, Zhang K, Chen Y, Li L, Liu X, Zheng J & Zhang Y, Inhibition of mild steel corrosion in hydrochloric acid using two novel pyridine Schiff base derivatives: A comparative study of experimental and theoretical results, *RSC Adv*, 7 (2017) 43014.
27 Khadijah N, Kamal M K M U, Fadzil A H, Kassim K, Rashid S H & Mastuli M S, Synthesis, characterization and corrosion inhibition studies of o, m, p-decanoylthiourea derivatives on mild steel in 0.1 M H_2SO_4 solutions, *Malay J Anal Sci*, 18 (2014) 21.
28 Pocker Y, Meany J E & Nist B J, Reversible hydration of 2-and 4-pyridinecarboxaldehydes. I. Equilibrium studies, *J Phys Chem*, 71 (1967) 4509.
29 Khaled K F, Electrochemical investigation and modeling of corrosion inhibition of aluminum in molar nitric acid using some sulphur-containing amines, *Corros Sci*, 52 (2010) 2905.
30 Djenane M, Chafaa S, Chafai N, Kerkour R & Hellal A, Synthesis, spectral properties and corrosion inhibition efficiency of new ethyl hydrogen [(methoxyphenyl) (methylamino) methyl] phosphonate derivatives: Experimental and theoretical investigation, *J Mol Struct*, 1175 (2019) 398.
31 Moumeni O, Mehri M, Kerkour R, Boublia A, Mihoub F, Rebai K, Khan A A, Erto A, Darwish A S, Lemaoui T, Chafai N & Benguerba Y, Experimental and detailed DFT/MD simulation of α-aminophosphonates as promising corrosion inhibitor for XC48 carbon steel in HCl environment, *J Taiwan Inst Chem Eng*, 147 (2023) 104918.
32 Ghosal P S & Gupta A K, Determination of thermodynamic parameters from Langmuir isotherm constant-revisited, *J Mol Liq*, 225 (2017) 137.
33 Cano E, Polo J L, La-Iglesia A & Bastidas J M, A study on the adsorption of benzotriazole on copper in hydrochloric acid using the inflection point of the isotherm, *Adsorption*, 10 (2004) 219.
34 Gewirth A A & Niece B K, Electrochemical applications of in situ scanning probe microscopy, *Chem Rev*, 97 (1997) 1129.
35 Moumeni O, Chafaa S, Kerkour R, Benbouguerra K & Chafai N, Synthesis, structural and anticorrosion properties of diethyl (phenylamino) methyl) phosphonate derivatives: Experimental and theoretical study, *J Mol Struct*, 1206 (2020) 127693.
36 Kerkour R, Moumeni O, El-houda-Rabhi N, Mehri M, Boublia A, Chafai N & Chafaa S, Synthesis, DFT investigation, ADME-T properties, molecular docking and molecular dynamics simulation of new α-aminophosphonate inhibitor targeting Mpro and RdRp enzymes in SARS-CoV-2, *J Mol Struct*, 1315 (2024) 138842.
37 Lukovits I, Kalman E & Zucchi F, Corrosion inhibitors-correlation between electronic structure and efficiency, *Corrosion*, 57 (2001) 3.
38 Gomez B, Likhanova N V, Dominguez-Aguilar M A, Martinez-Palou R, Vela A & Gazquez J L, *J Phys Chem B*, 110 (2006) e8928.
39 Guo L, Kaya S, Obot I B, Zheng X & Qiang Y, Toward understanding the anticorrosive mechanism of some thiourea derivatives for carbon steel corrosion: A combined DFT and molecular dynamics investigation, *J Colloid Interf Sci*, 506 (2017) 478.
40 Chugh B, Singh A K, Thakur S, Pani B, Lgaz H, Chung I M, Jha R & Ebenso E E, Comparative investigation of corrosion-mitigating behavior of thiadiazole-derived bis-schiff bases for mild steel in acid medium: Experimental, theoretical, and surface study, *ACS Omega*, 5 (2020) 13503.